

Released momentum distribution of a Fermi gas in the BCS-BEC crossover

M.L. Chiofalo¹, S. Giorgini^{2,3} and M. Holland²

¹*INFM and Classe di Scienze, Scuola Normale Superiore, Pisa, Italy*

²*JILA and Department of Physics, University of Colorado at Boulder, Boulder, CO 80309-0440, U.S.A*

³*Dipartimento di Fisica, Università di Trento and BEC-INFM, I-38050 Povo, Italy*

(Dated: June 24, 2018)

We develop a time-dependent mean-field theory to investigate the released momentum distribution and the released energy of an ultracold Fermi gas in the BCS-BEC crossover after the scattering length has been set to zero by a fast magnetic-field ramp. For a homogeneous gas we analyze the non-equilibrium dynamics of the system as a function of the interaction strength and of the ramp speed. For a trapped gas the theoretical predictions are compared with experimental results.

PACS numbers:

The study of the momentum distribution of an atomic gas in the quantum degenerate regime carries a wealth of information on the role played by interactions and on the existence of a superfluid order parameter. As an example, in a homogeneous Bose gas at $T = 0$, the momentum distribution $n_{\mathbf{k}}$ exhibits a singular behavior at small wave vectors $n_{\mathbf{k}} \simeq mc/2\hbar k$, which is determined by the excitation of phonons propagating with the speed of sound c and is a signature of Bose-Einstein condensation [1]. In a corresponding system of fermions with attractive interactions, the broadening of the Fermi surface is instead a consequence of the formation of pairs and of the presence of a superfluid gap [2]. This latter effect becomes dramatic in the BCS-BEC crossover region where the pairing gap is of the order of the Fermi energy of the system [3]. The second moment of the momentum distribution defines the kinetic energy of the system: $E_{kin} = \sum_{\mathbf{k}} n_{\mathbf{k}} \hbar^2 k^2 / (2m)$, where m is the mass of the atoms. This quantity, which also plays a central role in the many-body description of ultracold gases, is very sensitive to the large- k behavior of $n_{\mathbf{k}}$. For interacting systems the dominant contribution to E_{kin} comes from short-range correlations, where the details of the interatomic potential are relevant. In the case of a zero-range potential it is well known that the momentum distribution decreases like $1/k^4$ for large momenta and the kinetic energy diverges in dimensionality greater than one. This unphysical divergence can be understood recalling that the zero-range approximation is only correct to describe the region of momenta $k \ll 1/r_0$, where r_0 denotes the physical range of interactions [4]. This behavior of the kinetic energy is a general feature of quantum-degenerate gases, where interactions are well described by the s -wave scattering length a , holding both for fermions and bosons and for repulsive and attractive interactions [5].

The physics of ultracold gases is characterized by a clear separation of energy scales: the energy scale associated with the two-body physics as fixed for example by $\hbar^2/mr_0^2 \sim 10mK$, being $r_0 \sim 100a_0$ the typical interaction length of the Van der Waals potential, and the energy scale associated with the many-body physics as determined by the typical Fermi energy $\epsilon_F \sim 1\mu K$. This separation of energy scales provides a very large range of

timescales for which the dynamical process can be safely considered *fast* (*diabatic*) as the many-body dynamics is concerned and *slow* (*adiabatic*) with respect to the two-body dynamics. This feature is exploited in recent experiments aiming to measure the momentum distribution, that are based on the ballistic expansion of the cloud after the scattering length has been quickly set to zero by a fast magnetic-field ramp [6, 7]. These experiments give access to the released momentum distribution, which is a non-equilibrium quantity defined as the momentum distribution of the system after the scattering length has been rapidly ramped to $a = 0$. Provided the timescale of the ramp satisfies the conditions given above, the released momentum distribution does not depend on the detailed structure of the interatomic potential, being in this sense universal, but it does depend on the timescale of the ramping process. An important theoretical issue is to investigate the properties of the released momentum distribution and to understand what useful information about the system can be extracted from it.

In this Letter we calculate the released momentum distribution of a Fermi gas at $T = 0$ in the BCS-BEC crossover. We calculate the released momentum distribution and its second moment for a homogeneous system as a function of the interaction strength $1/(k_F a)$, where k_F is the Fermi wave vector. For harmonically trapped systems we give an explicit prediction of the column integrated released momentum distribution and of the released energy for values of the interaction strength ranging from the BCS to the BEC regime and we compare our results with recently obtained experimental data [7].

We consider an unpolarized two-component Fermi gas with equal populations of the \uparrow and \downarrow components: $N_{\uparrow} = N_{\downarrow} = N/2$, where N is the total number of particles. We determine the dynamical evolution of such a system starting from the equations of motion for the non-equilibrium density matrices of the \uparrow and \downarrow components interacting through the Hamiltonian

$$H = \sum_{\sigma} \int d\mathbf{x} \psi_{\sigma}^{\dagger}(\mathbf{x}) \left(-\frac{\hbar^2 \nabla_{\mathbf{x}}^2}{2m} \right) \psi_{\sigma}(\mathbf{x}) + \int d\mathbf{x} d\mathbf{x}' \psi_{\uparrow}^{\dagger}(\mathbf{x}) \psi_{\downarrow}^{\dagger}(\mathbf{x}') V(\mathbf{x}, \mathbf{x}') \psi_{\downarrow}(\mathbf{x}') \psi_{\uparrow}(\mathbf{x}) \quad (1)$$

where $\sigma = \uparrow, \downarrow$ labels the spins and $V(x, x')$ is the interaction potential to be specified later. The correlations are treated within a mean-field approach [3], where they are expressed in terms of the normal $G_{N\sigma}(\mathbf{x}, \mathbf{x}', t) = \langle \psi_\sigma^\dagger(\mathbf{x}', t) \psi_\sigma(\mathbf{x}, t) \rangle$ and the anomalous $G_A(\mathbf{x}, \mathbf{x}', t) = \langle \psi_\downarrow(\mathbf{x}', t) \psi_\uparrow(\mathbf{x}, t) \rangle$ density matrices. By neglecting the Hartree terms one obtains the following coupled equations of motion [2] (from now on $G_{N\uparrow}(\mathbf{x}, \mathbf{x}', t) = G_{N\downarrow}(\mathbf{x}, \mathbf{x}', t) \equiv G_N(\mathbf{x}, \mathbf{x}', t)$)

$$i\hbar \frac{dG_N(\mathbf{x}, \mathbf{x}', t)}{dt} = \left(-\frac{\hbar^2 \nabla_{\mathbf{x}}^2}{2m} + \frac{\hbar^2 \nabla_{\mathbf{x}'}^2}{2m} \right) G_N(\mathbf{x}, \mathbf{x}', t) + \int d\mathbf{x}'' [V(\mathbf{x}, \mathbf{x}'') - V(\mathbf{x}'', \mathbf{x}')] G_A(\mathbf{x}, \mathbf{x}'', t) G_A^*(\mathbf{x}'', \mathbf{x}', t) \quad (2)$$

and

$$i\hbar \frac{dG_A(\mathbf{x}, \mathbf{x}', t)}{dt} = \left(-\frac{\hbar^2 \nabla_{\mathbf{x}}^2}{2m} - \frac{\hbar^2 \nabla_{\mathbf{x}'}^2}{2m} \right) G_A(\mathbf{x}, \mathbf{x}', t) + V(\mathbf{x}, \mathbf{x}') G_A(\mathbf{x}, \mathbf{x}', t) - \int d\mathbf{x}'' V(\mathbf{x}, \mathbf{x}'') G_N(\mathbf{x}', \mathbf{x}'', t) G_A(\mathbf{x}, \mathbf{x}'', t) - \int d\mathbf{x}'' V(\mathbf{x}, \mathbf{x}'') G_N(\mathbf{x}, \mathbf{x}'', t) G_A(\mathbf{x}'', \mathbf{x}', t). \quad (3)$$

The short-range nature of the interaction potential $V(\mathbf{x}, \mathbf{x}')$ can be properly described through the regularized pseudopotential $V(\mathbf{r}) = (4\pi a \hbar^2 / m) \delta(\mathbf{r}) (\partial / \partial r) r$ [8], with a the s -wave scattering length and $r \equiv |\mathbf{x} - \mathbf{x}'|$. During the magnetic-field ramp the value of the scattering length changes in time according to the relation

$$a(t) = a_{bg} \left(1 - \frac{\Gamma}{B(t) - B_0} \right), \quad (4)$$

valid close to the Feshbach resonance. In the above expression, a_{bg} denotes the background scattering length, B_0 and Γ the position and width of the resonance respectively, and $B(t)$ is the instantaneous value of the magnetic field. Under the dynamical conditions that we are considering, where the non-equilibrium processes take place over a timescale adiabatic with respect to the two-particle problem and diabatic with respect to the many-particle system, the time evolution does not depend on the details of the short-range potential and the effect of interactions results in a boundary condition at short length scales

$$\left[\frac{(rG_A(r, t))'}{rG_A(r, t)} \right]_{r=0} = -\frac{1}{a(t)}, \quad (5)$$

where the prime indicates the derivative with respect to r , which must be fulfilled at any time t . For small values of r , many-body effects in Eq. (3) can be neglected and the boundary condition (5) corresponds to the one of the two-body problem with the pseudopotential $V(\mathbf{r})$, where $G_A(r, t)$ plays the role of the wave function for the relative motion. A similar argument is known to hold also in the electron gas, where one has the boundary condition

$[g'(r)/g(r)]_{r=0} = 1/a_B$ for the pair correlation function $g(r)$ (a_B is the Bohr radius), referred to as the Kimball relation [9].

In the case of a homogeneous system and by using the pseudopotential approximation for the interatomic potential $V(\mathbf{x}, \mathbf{x}'')$ and the boundary condition (5), Eqs. (2)-(3) can be greatly simplified. For example, the term $\int d\mathbf{x}'' V(\mathbf{x}, \mathbf{x}'') G_N(\mathbf{x}', \mathbf{x}'', t) G_A(\mathbf{x}, \mathbf{x}'', t)$ in Eq. (3) becomes $(4\pi \hbar^2 a / m) G_N(r, t) [(rG_A)']_{r=0} = -(4\pi \hbar^2 / m) G_N(r, t) [(rG_A)]_{r=0}$, where we have also used the fact that the short ranged $V(\mathbf{x}, \mathbf{x}'')$ picks up the $\mathbf{x}'' = \mathbf{x}$ value of $G_N(\mathbf{x}', \mathbf{x}'', t)$. After dealing with the other terms in a similar way, we obtain the simpler coupled equations for $\tilde{G}_N(r, t) \equiv rG_N(r, t)$ and $\tilde{G}_A(r, t) \equiv rG_A(r, t)$

$$i\hbar \frac{d\tilde{G}_N(r, t)}{dt} = \frac{8\pi \hbar^2}{m} i\Im \left(\tilde{G}_A(r, t) [\tilde{G}_A^*(t)]_{r=0} \right) \quad (6)$$

$$i\hbar \frac{d\tilde{G}_A(r, t)}{dt} = -\frac{\hbar^2 \partial^2}{m \partial r^2} \tilde{G}_A(r, t) + \frac{8\pi \hbar^2}{m} \tilde{G}_N(r, t) [\tilde{G}_A(t)]_{r=0}, \quad (7)$$

with the boundary condition $[(\tilde{G}_A)'/\tilde{G}_A]_{r=0} = -1/a(t)$. Notice that interaction effects only enter Eqs. (6)-(7) through the boundary condition (5). We determine the initial conditions $\tilde{G}_N(r, t=0)$ and $\tilde{G}_A(r, t=0)$ of Eqs.(6)-(7) from the mean-field gap and number equations corresponding to the equilibrium state of the gas with the initial value of the scattering length $a(0)$

$$n = \int_0^\infty \frac{dk k^2}{2\pi^2} \left(1 - \frac{\epsilon_k - \mu}{\sqrt{(\epsilon_k - \mu)^2 + \Delta^2}} \right) \quad (8)$$

$$\frac{m}{4\pi \hbar^2 a(0)} = \int_0^\infty \frac{dk k^2}{4\pi^2} \left[\frac{1}{\epsilon_k} - \frac{1}{\sqrt{(\epsilon_k - \mu)^2 + \Delta^2}} \right] \quad (9)$$

where $\epsilon_k = \hbar^2 k^2 / 2m$, μ is the chemical potential, Δ the superfluid gap and $n = n_\uparrow + n_\downarrow$ the total particle density. The functions \tilde{G}_N and \tilde{G}_A are then calculated from the Bogoliubov quasiparticle amplitudes

$$u_k^2 = 1 - v_k^2 = \frac{1}{2} \left(1 + \frac{\epsilon_k - \mu}{\sqrt{(\epsilon_k - \mu)^2 + \Delta^2}} \right), \quad (10)$$

as

$$\tilde{G}_N(r, t=0) = \frac{1}{2\pi^2} \int_0^\infty dk k \sin(kr) v_k^2 \quad (11)$$

and

$$\tilde{G}_A(r, t=0) = \frac{1}{2\pi^2} \int_0^\infty dk k \sin(kr) u_k v_k. \quad (12)$$

We solve the dynamic equations (6)-(7) with the initial conditions (11)-(12) and $a(t)$ given by (4) from the initial time $t=0$ to the final time $t=t_f$, where $a(t_f)=0$. The

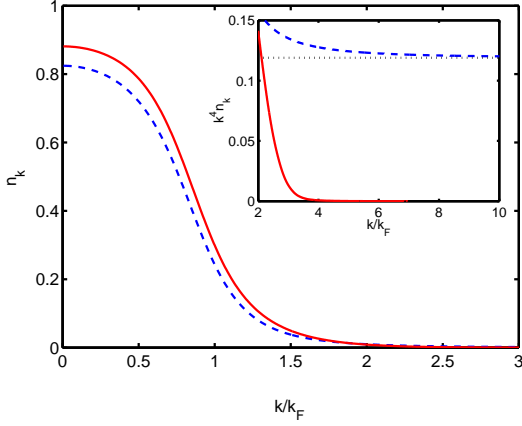


FIG. 1: (color online) Released momentum distribution (solid lines) of a homogeneous gas at unitarity, $1/(k_F a(0)) = 0$, for a ramp rate of $2\mu\text{s/G}$. The large- k behavior of n_k weighted by k^4 is shown in the inset, where the dotted line corresponds to the equilibrium asymptotic value $(\Delta/2\epsilon_F)^2$. The initial equilibrium distribution is also shown (dashed lines).

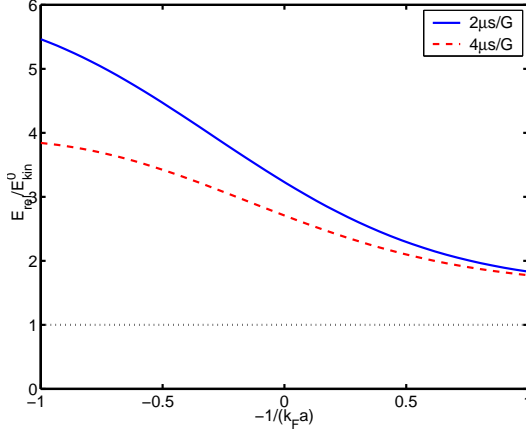


FIG. 2: (color online) Released energy as a function of the interaction strength for two values of the ramp rate. The energy is normalized to the kinetic energy of the non-interacting gas $E_{kin}^0 = 3\epsilon_F/8$.

released momentum distribution is then calculated from the Fourier transform of G_N at the time $t = t_f$

$$n_{\mathbf{k}}(t = t_f) = \int d\mathbf{r} e^{i\mathbf{k}\cdot\mathbf{r}} G_N(\mathbf{r}, t = t_f). \quad (13)$$

The results for the homogeneous gas are shown in Figs. 1-2. In Fig. 1 we compare the equilibrium momentum distribution $n_{\mathbf{k}}(t = 0)$ in the unitary limit, $1/(k_F a(0)) = 0$, with the corresponding released momentum distribution (13) calculated for a magnetic-field ramp rate of $2\mu\text{s/G}$. For values of $k \lesssim k_F$ the shape of the distribution does not change appreciably. The large- k tail is instead greatly suppressed (as is shown in the

inset) and the second moment of the released $n_{\mathbf{k}}$ is a convergent integral. Notice that the fast decaying tail of the released $n_{\mathbf{k}}$ affects the normalization constant. In Fig. 2 we show the results of the released energy as a function of the initial interaction strength $1/(k_F a(0))$ for two different values of the magnetic-field ramp rate. We notice that on the BCS side of the crossover, $k_F a(0) < 0$, the dependence on the ramp rate is weak, while on the BEC side, $k_F a(0) > 0$, a faster ramp produces a significantly larger energy. In the BEC regime the system is in fact more sensitive to changes of the high-energy tail of the momentum distribution. Deep in the BCS regime, $-1/(k_F a(0)) \gg 1$, the released energy reduces to the kinetic energy of the non-interacting gas $E_{kin}^0 = 3\epsilon_F/8$. In the opposite BEC regime, $-1/(k_F a(0)) \ll -1$, many-body effects become less relevant and the released energy coincides with the one obtained from the dissociation of the molecular state [7] (see Fig. 4).

In order to make quantitative comparison with the experiment, we now consider harmonically trapped systems confined by the external potential $V_{ext}(\mathbf{r}) = m(\omega_x^2 x^2 + \omega_y^2 y^2 + \omega_z^2 z^2)/2$. Within the local density approximation (LDA) we introduce the rescaled spatial variables $\tilde{x} = x\sqrt{\omega_x/\omega}$, $\tilde{y} = y\sqrt{\omega_y/\omega}$ and $\tilde{z} = z\sqrt{\omega_z/\omega}$, so that the confining potential becomes isotropic in the new coordinates $V_{ext}(\mathbf{r}) = m\omega^2 \tilde{R}^2/2$, where $\omega = (\omega_x \omega_y \omega_z)^{1/3}$ is the geometric average of the harmonic oscillator frequencies. For each spatial slice $\tilde{\mathbf{R}} = (\tilde{\mathbf{x}} + \tilde{\mathbf{x}}')/2$, Eqs. (8)-(9) are solved for the local chemical potential $\mu_{local}(\tilde{\mathbf{R}})$ and the local density $n(\tilde{\mathbf{R}})$, subject to the normalization $\int d^3\tilde{\mathbf{R}} n(\tilde{\mathbf{R}}) = N$ and the local equilibrium condition $\mu = \mu_{local}(\tilde{\mathbf{R}}) + V_{ext}(\tilde{\mathbf{R}})$. Each slice is then evolved according to Eqs. (6)-(7) with initial conditions $\tilde{G}_N(\tilde{r}, \tilde{R}, t = 0)$ and $\tilde{G}_A(\tilde{r}, \tilde{R}, t = 0)$, where $\tilde{r} = \tilde{\mathbf{x}} - \tilde{\mathbf{x}}'$ is the relative coordinate. The released momentum distribution is obtained from $G_N(\tilde{r}, \tilde{R}, t)$ at the final time $t = t_f$ through the integral over the rescaled coordinates $\tilde{\mathbf{R}}$ and $\tilde{\mathbf{r}}$,

$$n(k, t = t_f) = \int d^3\tilde{\mathbf{R}} \int d^3\tilde{\mathbf{r}} e^{i\mathbf{k}\cdot\tilde{\mathbf{r}}} G_N(\mathbf{r}, \mathbf{R}, t = t_f). \quad (14)$$

In Fig. 3 we compare the column integrated released momentum distribution $n(\sqrt{k_x^2 + k_y^2}, t_f) = \int_{-\infty}^{\infty} dk_z n(k, t_f)$, calculated from Eq. (14), with the experimental results obtained in Ref. [7]. The values of the interaction strength are $1/(k_F^0 a(0)) = -0.66, 0$ and 0.59 as in the experiments and the magnetic-field ramp rate is $2\mu\text{s/G}$. The agreement is quite good for the momentum distribution on the BEC side of the resonance and in the unitary limit. On the BCS side of the resonance the experimental $n(k)$ is more broadened because the Hartree mean-field term, which enhances the shrinking of the cloud due to attraction, is neglected in the calculation. In Fig. 4 we show the results for the released energy of the inhomogeneous gas as a function of the interaction strength $1/(k_F^0 a(0))$, where $k_F^0 = (24N)^{1/6} \sqrt{m\omega/\hbar}$ is the

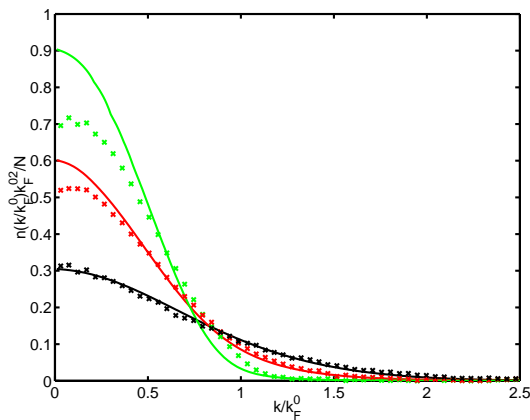


FIG. 3: (color online) Column integrated released momentum distribution of a harmonically trapped gas. From top to bottom, the lines correspond to $1/(k_F^0 a(0)) = -0.66$ (green), $1/(k_F^0 a(0)) = 0$ (red) and $1/(k_F^0 a(0)) = 0.59$ (black). The magnetic-field ramp rate is $2\mu\text{s/G}$. The symbols correspond to the experimental results of Ref. [7].

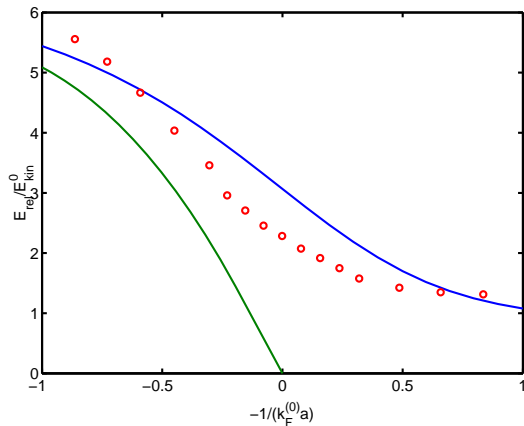


FIG. 4: (color online) Released energy of a harmonically trapped gas as a function of the interaction strength $1/(k_F^0 a(0))$ for a ramp rate of $2\mu\text{s/G}$ (upper blu line). The lower (green) line is the corresponding result solving the two-body problem associated with the molecular state. The symbols are the experimental results from Ref. [7]. The energy is normalized to the kinetic energy of the non-interacting gas $E_{kin}^0 = 3\epsilon_F^0/8$.

Fermi wave vector in the center of the trap corresponding to a non-interacting gas. Experimental results from Ref. [7] and theoretical results obtained by solving the time-dependent Schrödinger equation for the molecular

state (see [7]) are also shown in Fig. 4. The full many-body calculation reduces to the molecular two-body result only in the deep BEC regime, $-1/k_F^0 a(0) \ll -1$, and agrees better with the experimental results. Considering that there are no adjustable parameters in the comparison between theory and experiment, the agreement is remarkable over the whole crossover region. In the unitary limit the mean-field approach employed in the present study is known to overestimate the equilibrium energy per particle compared to more advanced quantum Monte Carlo calculations [10]. This might be the reason for the larger energy obtained around resonance compared to the observed one. Furthermore, on the BCS side of the resonance, the present approach neglects the mean-field Hartree term and we expect a faster convergence to the kinetic energy of the non interacting gas $E_{kin}^0 = 3\epsilon_F^0/8$, where $\epsilon_F^0 = (\hbar k_F^0)^2/2m$, as $-1/k_F^0 a(0)$ becomes large. A more sophisticated time-dependent theory is needed to improve the quantitative agreement with experiments.

In conclusion, we have developed a time-dependent mean-field scheme which allows one to calculate the released momentum distribution and the released energy of a Fermi gas in the BCS-BEC crossover if the scattering length is set to zero using a fast magnetic-field ramp. Our analysis clarified that the dynamical effects due to the magnetic-field ramp suppress the high-energy tail of the momentum distribution. For harmonically trapped systems we compared our theoretical predictions with the recently obtained experimental results of Ref. [7]. Qualitatively we reproduced the data well, but significant quantitative discrepancies are found. The underestimate of the release energy of the theory compared to experiment on the deep BCS side is anticipated due to the neglect of the Hartree energies. On the deep BEC side, the underestimate may be due to the effect of finite temperature on the experimental data in that regime. The significant overestimate of the release energy at resonance is more difficult to explain and may indicate the inadequacy of the Leggett ground state form for describing the gas in the unitary limit. This would illustrate a need to include correlations beyond the pair correlations given in the Cooper pair picture in order to explain the observed experimental expansion energetics on resonance.

Acknowledgements: SG acknowledges support by the Ministero dell'Istruzione, dell'Università e della Ricerca (MIUR) and from the National Science Foundation. MH acknowledges support from the U.S. Department of Energy, Office of Basic Energy Sciences via the Chemical Sciences, Geosciences and Biosciences Division.

-
- [1] See *e.g.* L.P. Pitaevskii and S. Stringari, *Bose-Einstein Condensation* (Oxford University Press, Oxford, 2003).
 - [2] See *e.g.* P.G. de Gennes, *Superconductivity of Metals and*

Alloys (Addison-Wesley, California, 1966).

- [3] A.J. Leggett, in *Modern Trends in the Theory of Condensed Matter*, edited by A. Pekalski and R. Przys-

- tawa (Springer-Verlag, Berlin, 1980); P. Nozières and S. Schmitt-Rink, J. Low Temp. Phys. **59**, 195 (1985); J.R. Engelbrecht, M. Randeria and C.A.R. Sá de Melo, Phys. Rev. B **55**, 15153 (1997).
- [4] E.E. Nikitin and L.P. Pitaevskii, preprint cond-mat/0508684.
- [5] At $T = 0$ for a Bose gas with repulsive interactions one finds $n_{\mathbf{k}} \simeq 1/(16k^4\xi^4)$ at large momenta, where $\xi = 1/\sqrt{8\pi na}$ is the healing length with n the particle density and a the s -wave scattering length. For a Fermi gas one finds instead $n_{\mathbf{k}} \simeq m^2\Delta^2/(\hbar^4k^4)$, where Δ is the BCS gap, for attractive interactions and $n_{\mathbf{k}} \simeq (4ak_F/3\pi)^2(k_F/k)^4$ for repulsive interactions [V.A. Belyakov, Sov. Phys. JETP **13**, 850 (1961)].
- [6] T. Bourdel *et al.*, Phys. Rev. Lett. **91**, 020402 (2003).
- [7] C.A. Regal *et al.*, Phys. Rev. Lett. **95**, 250404 (2005).
- [8] G. Bruun, Y. Castin, R. Dum and K. Burnett, Eur. Phys. J. D **7**, 433 (1999).
- [9] J.-C. Kimball, Phys. Rev. A **7**, 1648 (1973); G. Niklasson, Phys. Rev. B **10**, 3052 (1974).
- [10] J. Carlson, S.-Y. Chang, V.R. Pandharipande and K.E. Schmidt, Phys. Rev. Lett. **91**, 050401 (2003), G.E. Astrakharchik, J. Boronat, J. Casulleras and S. Giorgini, Phys. Rev. Lett. **93**, 200404 (2004).